Soft Matter

PAPER

View Article Online
View Journal | View Issue

Cite this: *Soft Matter*, 2019, **15**, 8611

Neutralisation rate controls the self-assembly of pH-sensitive surfactants†

Dominic W. Hayward, *[ab] Leonardo Chiappisi, [ab] Jyh Herng Teo,[b] Sylvain Prévost, [b] Ralf Schweins[b] and Michael Gradzielski *[a]

Received 9th May 2019,
Accepted 1st October 2019

DOI: 10.1039/c9sm00950g

rsc.li/soft-matter-journal

The degree of ionisation of a weakly acidic surfactant can be continuously modified from nonionic to ionic by adjusting the pH. This property can be used to control the curvature and therefore the morphology of the self-assembled aggregates it forms in solution. Herein, we report the surprising phenomenon, observed in the alkyl ether oligo(ethylene oxide) carboxylate ($CH_3(CH_2)_{11/13}OEO_{4.5}CH_2COOH$), whereby it is not only the pH but also the neutralisation rate that affects the aggregate morphology. Specifically, when the pH is increased slowly, up to 40 wt% of the surfactant remains in a long-lived vesicle state at high pH. This phenomenon was characterised in detail by small-angle neutron scattering and light scattering techniques. The cause of this phenomenon is thought to be related to a combination of polydispersity and the formation of acid-carboxylate dimers close to the pK_a. The transition of these vesicles to the thermodynamically favoured micelles at high pH is inhibited by a high activation energy barrier and therefore only occurs very slowly. Increasing the NaCl concentration eliminates the presence of vesicles at high pH, demonstrating that the activation energy for the vesicle-to-micelle transition depends strongly on electrostatic interactions. These experiments show that the preparation pathway can be used to obtain different self-assembled structures at identical conditions *via* kinetic control. This phenomenon provides a useful tool for devising formulations where the properties of the system can be altered without changing the composition.

1 Introduction

Surfactants are low molecular weight amphiphiles that spontaneously self-assemble in aqueous solution. Depending on their chemical structure and environment, they can form a variety of different aggregate morphologies ranging from spherical and cylindrical micelles to planar lamellae and vesicles.[1] The most common equilibrium morphology is that of spherical micelles and equilibration is generally achieved rapidly – typically in the millisecond to second regime. The kinetics of micelle formation are often described using two time constants, where the faster is associated with the exchange of single surfactant molecules and the slower with the complete disintegration of the aggregates.[2] One therefore generally expects that micelles composed of low molecular weight surfactants will be in an equilibrated state shortly after their preparation or after a change of the solution conditions, such as temperature, pH or ionic strength.

In the case of vesicles, which are much larger in size and have much higher aggregation numbers, formation *via* stepwise addition of individual molecules is statistically extremely unlikely. The kinetic processes that govern aggregation and disintegration are therefore rather different and in many cases difficult to elucidate precisely. In one system where the mechanism has been studied in detail, vesicle formation occurs *via* the growth of disklike micelles which then fuse and subsequently close into a spherical form.[3–5] This process takes place on a timescale ranging from seconds to several hours, depending on the type of amphiphile present, and may be controlled by the addition of adulterants such as polymer surfactants, which act to stabilise the disc rims.[6] Other vesicle transformation or ageing processes have been reported with equilibration times from a few days up to several months.[7–9]

The spontaneous formation of stable, or at least metastable, vesicles in single component surfactant solutions is uncommon and, for the most part, restricted to double-tailed molecules.[10–12] Recently, spontaneous vesicle formation has also been reported in single-chain surfactants with phosphate[13,14] or carboxylate headgroups.[15–17] In this case, it is thought that the vesicles are composed of acid-soap dimers, whereby surfactant molecules with protonated and monoanionic headgroups undergo hydrogen bonding to form dimers with a single negative charge. Such systems are

[a] *Stranski-Laboratorium für Physikalische und Theoretische Chemie, Institut für Chemie, Technische Universität Berlin, Straße des 17. Juni 124, D-10623 Berlin, Germany. E-mail: hayward@ill.fr, michael.gradzielski@tu-berlin.de*
[b] *Institut Laue-Langevin, 71 avenue des Martyrs, CS 20156, 38042 Grenoble cedex 9, France*

† Electronic supplementary information (ESI) available. See DOI: 10.1039/c9sm00950g

of interest, as the size and type of the aggregates depend both on the concentration of the surfactant[14,15] and the pH of the solution,[13,16–18] and could therefore be tuned to suit particular formulations or applications.

One such surfactant class, in which spontaneous vesicle formation has been observed, is the alkyl ether carboxylic acids (AECs). AECs are single-chained, weakly anionic surfactants with carboxylate head-groups. They are used in cosmetic and detergent formulations[19] as well as in oil extraction techniques[20] and are therefore industrially relevant and widely available. Of particular interest with regards to its self-assembly behaviour, is oligo-oxyethylene(4.5) lauryl ether carboxylic acid, which forms a mixture of vesicles and micelles at low pH (approx. 3–5)[17,18] and exclusively micelles at high pH. As a result of this relatively well-known pH-responsive behaviour, this surfactant was previously used to test the concept of an *in situ* chemical reactor sample environment for small-angle neutron scattering (SANS) experiments.[21] Here, in order to maximise the signal-to-noise ratio, particularly for the low-Q measurements, the pH of the aqueous surfactant solution was adjusted very slowly compared to the previous experiments (10 mL of 0.1 M NaOH added over 120 minutes *vs.* 0.1 mL of 10 M NaOH added over 1 s). In this case, a small fraction ($\sim$1–2 wt%) of larger structures persisted in solution, even at high pH ($\sim$10). Repeat measurements of the same samples after 24 hours yielded the same results, indicating that the resulting structures are at least metastable with respect to the expected dynamics of small-molecule, surfactant-based micelles. The results observed in ref. 21 are notable for two reasons: firstly, it is rather unusual to have two distinct, coexisting populations with different morphologies arising from a single type of surfactant molecule in solution. Secondly, pathway-dependent self-assembly is rare in simple surfactant systems.

As it was not clear how and why this type of complex behaviour should manifest in such an ostensibly simple system, this work has been undertaken to confirm that the effect is real (*i.e.* not an artefact arising from a particular measurement technique or a contaminated sample), to elucidate the effect in detail and to establish a possible mechanism. This study contains a detailed investigation on the effects of base addition-rate on the self-assembly behaviour of AECs with respect to: surfactant composition, base concentration, base composition and salt concentration. The results confirm the complexity of the phenomenon and are discussed in relation to possible explanations and potential routes by which this behaviour may be exploited.

2 Experimental

2.1 Materials

The surfactants AKYPO RLM 45 CA ($C_{12}E_5Ac$) and AKYPO RO 50 VG ($C_{18:1}E_5Ac$) were kindly donated by Kao Chemicals GmbH (Emmerich, Germany) and the surfactant NIKKOL ECT-7 ($C_{13}E_7Ac$) was donated by Nikko Chemicals (Tokyo, Japan). A generalised chemical structure of the surfactants is provided in Fig. 1 and the specific chemical structures of the individual materials is give in Fig. S1 in the ESI.† The nomenclature

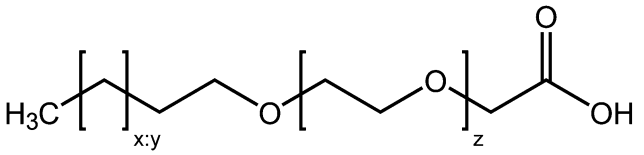

Fig. 1 Generalised chemical structure of the surfactants used in this work. The surfactants differ from each other in three ways: the length of the alkyl chain (x), the number of double bonds in the alkyl chain (y) and the number of ethylene oxide units (z). The approximate structures of the individual materials are provided in Fig. S1 (ESI†).

used in the abbreviations derives from that used for fatty acids, so the material $C_{x:y}E_zAc$ comprises: an alkyl chain with x carbons and y double bonds, a single oxygen followed by z ethylene oxide units and a CH_2COOH carboxymethyl termination. As it may be relevant for the phenomena described in this work, it is instructive to briefly consider what is known about the composition of these materials. The surfactants are all produced in industrial quantities and are polydisperse in both alkyl chain length and number of ethylene oxide units. Molecules of AKYPO RLM 45 CA may have one of three different alkyl chain lengths (C_{12}, C_{14} and C_{16}) in the approximate ratio 2 : 1 : 0.25 and a distribution of ethylene oxide units centred around 4.5. Molecules of AKYPO RO 50 VG have alkyl chains $C_{18:1}$ or C_{16} in the ratio 3 : 1 and an ethylene oxide distribution centred around 5 units. Molecules of NIKKOL ECT-7 have alkyl chains of length C_{12}, C_{13} or C_{14} in the ratio 2 : 3 : 2 and an ethylene oxide distribution centred around 7 units. Finally, due to the manner in which they are synthesised, the conversion from the ethoxylated alcohol to the carboxylic acid form may not be complete. The fraction of non-carboxymethylated chains is estimated to be approximately 10%.[18,22,23] The materials were characterised by electrospray ionisation mass spectrometry (ESI-MS) (see Fig. S2, ESI†) and inductively coupled plasma optical emission spectrometry (ICP-OES) and unless otherwise stated, used as received. A summary of the materials used is given in Table 1. Sodium hydroxide, potassium hydroxide and sodium chloride were obtained from Sigma Aldrich (St. Louis, USA) and used as received. The D_2O (>99.9%D) used for the preparation of samples for the SANS experiments was obtained from Euriso-top (Saint-Aubin, France).

2.1.1 Sample preparation. Aqueous stock solutions of surfactant were prepared at 1 wt% (equating to molar concentrations of 22.5 mM, 18.4 mM and 17.6 mM for $C_{12}E_5Ac$, $C_{13}E_7Ac$, and $C_{18:1}E_5Ac$ respectively), using ultrapure, deionised water (Milli-Q, 18.2 MΩ cm). With the exception of the 'reverse-addition' sample, all high pH samples were prepared in the same manner: a 40 mL vial was charged with 20 g of surfactant solution, the base (either NaOH or KOH) was added continuously *via* a syringe pump (33 DDS, Harvard Apparatus, USA) at the addition rates detailed in Table 2. For the 'reverse addition' sample, 0.5 mL of 1 M NaOH was added to 19.8 g deionised water in one portion, stirred for 5 minutes after which time, 0.2 g of unadulterated surfactant was added dropwise to the stirring solution. In the case of the salt-containing stock solutions, unless otherwise stated, the salt was added prior to

Table 1 Summary of the surfactants used in this work, according to the information provided by the manufacturers

Commercial name	Short form	Chemical formula[a]	Molecular weight (g mol^{-1})	Active matter
AKYPO RLM 45 CA	$C_{12}E_5Ac$	$CH_3(CH_2)_{11/13}OEO_{4.5}CH_2COOH$	444	92%
AKYPO RO 50 VG	$C_{18:1}E_5Ac$	$CH_3(CH_2)_{15/17:1}OEO_5CH_2COOH$	544	91%
NIKKOL ECT-7	$C_{13}E_7Ac$	$CH_3(CH_2)_{12}OEO_7CH_2COOH$	567	Not given
Brij L4	$C_{12}E_4OH$	$CH_3(CH_2)_{12}OEO_4H$	362	Not given

[a] In the chemical formulae, EO = –(CH_2CH_2O)– has been used.

Table 2 Summary of the concentrations, volumes and addition rates of NaOH and KOH used in this work. Each row represents a separate sample *i.e.* the amount of base added is identical in each case

				Equivalent addition rate ($mol_{base}/mol_{surfactant}/s$)		
Base concentration (mol L^{-1})	Volume (mL)	Addition time (s)	Addition rate (mol s^{-1})	$C_{12}E_5Ac$	$C_{13}E_7Ac$	$C_{18:1}E_5Ac$
0.1	5	8	6.25×10^{-5}	2.78×10^{-3}		
0.1	5	60	8.33×10^{-6}	3.70×10^{-4}		
0.1	5	600	8.33×10^{-7}	3.70×10^{-5}		
0.1	5	6000	8.33×10^{-8}	3.70×10^{-6}		
0.1	5	60 000	8.33×10^{-9}	3.70×10^{-7}		
0.1	5	600 000	8.33×10^{-10}	3.70×10^{-8}		
1	0.5	8	6.25×10^{-5}	2.78×10^{-3}	3.40×10^{-3}	3.55×10^{-3}
1	0.5	60	8.33×10^{-6}	3.70×10^{-4}		
1	0.5	600	8.33×10^{-7}	3.70×10^{-5}		
1	0.5	6000	8.33×10^{-8}	3.70×10^{-6}	4.53×10^{-6}	4.73×10^{-6}
1	0.5	60 000	8.33×10^{-9}	3.70×10^{-7}		
1	0.5	600 000	8.33×10^{-10}	3.70×10^{-8}		
10	0.05	8	6.25×10^{-5}	2.78×10^{-3}		
10	0.05	60	8.33×10^{-6}	3.70×10^{-4}		
10	0.05	600	8.33×10^{-7}	3.70×10^{-5}		
10	0.05	6000	8.33×10^{-8}	3.70×10^{-6}		

the surfactant and the high-pH solutions were then prepared as previously.

2.2 Small-angle neutron scattering (SANS)

SANS measurements were carried out on the D11 instrument at the Institut Laue-Langevin (ILL) in Grenoble.[24] Experiments were performed with a neutron wavelength of 6 Å and a path length of 2 mm at three sample-to-detector distances (SD): 1.5 m, 8 m and 39 m, covering the Q-range: 0.002–0.42 Å^{-1}. Absolute intensities were obtained with reference to the secondary calibration standard, H_2O (1 mm path length), which has a differential scattering cross-section of 0.983 cm^{-1} on the D11 instrument at λ = 6.0 Å. The raw data are available in the ILL data repository.[25] For each measurement, the 2D detector data were integrated over the azimuthal angle (0–2π), and the D_2O background was subtracted. Curves from the same sample at different SD were then combined and rebinned (the protocol for the rebinning algorithm is given in the ESI†). Finally, the data were fitted, in absolute units, to a two-component model[18,21] consisting of a population of ellipsoidal core–shell micelles (interacting *via* a charged hard sphere structure factor) and a population of non-interacting, unilamellar, core–shell vesicles. A mass balance constraint ensured that all of the surfactant material known to be present in the sample is in either one or the other of these aforementioned aggregation states. Details of the model, are given elsewhere[21] and the parameters used are given in the ESI.† At this point, it should be noted that, due to the existence of two polydisperse populations and the small weight fraction of the larger aggregates, the exact morphology of these aggregates could not be conclusively determined. However, as vesicles are known to exist at low pH[16,18] and the small-angle scattering has previously been observed to vary continuously with increasing pH,[21] consistent with a growing population of micelles and a shrinking population of vesicles, the description of the larger aggregates as vesicles has been adopted in this work.

2.3 Light scattering

Static and dynamic light scattering experiments (SLS and DLS respectively) were conducted concurrently using an ALV light scattering instrument consisting of a CGS-3 goniometer, a HeNe laser operating at a wavelength of 632.8 nm and an LSE 5004 digital correlator. Prior to measurement, all samples were filtered using mixed cellulose ester membrane filters (Millipore Millex-AA, Merck Millipore Ltd, 0.8 μm pore size) to remove large dust particles. Measurements were performed in cylindrical cells (8 mm inner diameter) at 25 °C for scattering angles between 30° and 150°, covering the Q-range: 6×10^{-4}–2.6×10^{-3} Å^{-1}. For the SLS measurements, absolute intensities were obtained with reference to the toluene standard using the Rayleigh ratio 1.340×10^{-5} cm^{-1}.

The autocorrelation functions resulting from the DLS measurements were analysed using two methods: an indirect Laplace transformation of the correlation function to give a continuous size distribution,[26] as well as a direct fit of the first-order field autocorrelation function using a double-exponential

model to extract the decay constants.[27] The field autocorrelation function $g^{(1)}$ was derived from the measured intensity autocorrelation function $g^{(2)}$ *via* the Siegert equation:[28]

$$g^{(2)} = 1 + \beta|g^{(1)}|^2 \quad (1)$$

where β is the coherence factor, related to the set-up of the instrument.

3 Results

3.1 SANS

In order to verify the reproducibility of the addition-rate dependence effect, a fresh batch of $C_{12}E_5Ac$ surfactant was used. Additionally, to investigate whether this effect also arises in other, analogous, AEC systems, two further surfactants were investigated: $C_{18:1}E_5Ac$ and $C_{13}E_7Ac$. Surfactant solutions were prepared at 1 wt% in D_2O, to which 0.5 mL of 1 M NaOD was added over either 8 seconds or 100 minutes (hereafter referred to as 'fast' and 'slow' additions respectively). As the number of molecules varied slightly between the different samples and surfactants used, an 'equivalent addition rate' was defined as the number of moles of base added per number of moles of surfactant present in solution per second (*i.e.* molar equivalents per second). The values are tabulated in Table 2. In addition, to investigate whether the effect could be attributed to irreversible chemical changes occurring in the surfactant as a result of reactions with the concentrated base, *via* alkaline hydrolysis for example, a sample was prepared in which the base was added prior to the surfactant. After initial measurements at 25 °C, all samples were also heated to 60 °C for 20 minutes, cooled to 25 °C and then remeasured. This was done in order to ascertain whether the self-assembled structures could be thermally 'annealed' into a thermodynamically favourable state. The resulting azimuthally-averaged scattering patterns are shown in Fig. 2(a–c), where the darker squares represent the initial measurements at 25 °C and the lighter triangles (almost entirely obscured behind the 25 °C data) represent the thermally 'annealed' samples. The parameters resulting from a non-linear least squares fit of the data to the two component model (consisting of ellipsoidal micelles and unilamellar vesicles), are given in Table 3. A comparison of the scattering patterns from the previous batch of $C_{12}E_5Ac$ and the batch used in this work is shown in Fig. S3 (ESI†). The scattering patterns from both batches are identical.

It is evident that the addition-rate effect for $C_{12}E_5Ac$ is also present in the new sample and is not simply an artefact arising from a particular batch. The fit parameters show that the weight fraction of surfactant in vesicle form is over an order of magnitude higher for the slow-addition sample with respect to the fast-addition sample. This difference remains after the samples have been heated and cooled, which suggests that the structures formed are kinetically stable with respect to temperature (see Fig. 2). Scattering from the 'reverse addition' sample was very similar to the sample prepared by fast addition, suggesting that the differences in nanostructure cannot be ascribed to locally high base concentrations hydrolysing the surfactant during the addition.

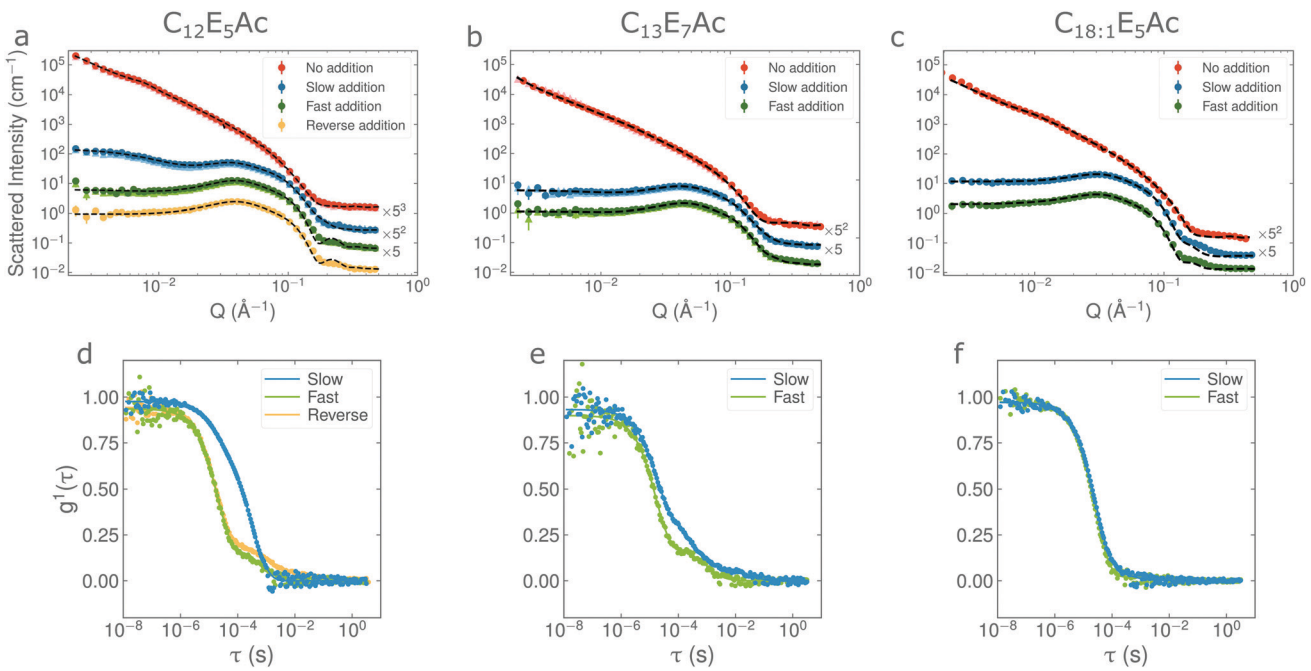

Fig. 2 Azimuthally averaged SANS data from 1 wt% solutions of (a) $C_{12}E_5Ac$, (b) $C_{13}E_7Ac$, (c) $C_{18:1}E_5Ac$. For each sample the darker circles indicate the scattering prior to heating and the lighter triangles indicate the scattering after heating (note that the data are so similar that the triangles are almost entirely obscured by the overlying circles). The dashed black lines are fits to the model described in the text. The data in (d) shows the azimuthally averaged scattering from 1 wt% solutions of $C_{12}E_5Ac$ that have received 2 additions of NaOD (slow-fast *vs.* fast-slow) either side of an addition of DCl. The 'slow' addition rates were 2.78×10^{-3}, 3.40×10^{-3} and 3.55×10^{-3} eq. s^{-1} and the fast addition rates were: 3.70×10^{-6}, 4.53×10^{-6} and 4.73×10^{-6} eq. s^{-1} for $C_{12}E_5Ac$, $C_{13}E_7Ac$ and $C_{18:1}E_5Ac$ respectively.

Table 3 Summary of the fit results for the SANS data shown in Fig. 2 after the addition of NaOH (*i.e.* at high pH). The radius of gyration of the micelle cores is given by $R_g = \sqrt{1/5 \cdot (a^2 + 2b^2)}$ where a and b are the semi-minor and semi-major axes of the ellipsoid. With the exception of $C_{12}E_5Ac$ slow addition sample, it was not possible to determine the vesicle radius with any degree of accuracy, as the weight fraction of surfactant in vesicle form was simply too low. For the purposes of comparing the fraction of surfactant in vesicle form, the vesicle radius was fixed at this value for all remaining fits. DLS measurements (see, for example, Fig. 3) show that this approximation is not unreasonable. All samples were prepared in D_2O, with 1 M NaOD. The 'slow' addition rates were: 2.78×10^{-3}, 3.40×10^{-3} and 3.55×10^{-3} eq. s^{-1} and the fast addition rates were: 3.70×10^{-6}, 4.53×10^{-6} and 4.73×10^{-6} eq. s^{-1} for $C_{12}E_5Ac$, $C_{13}E_7Ac$ and $C_{18:1}E_5Ac$ respectively. For the reverse addition sample, the base was added prior to the drop-wise addition of surfactant. Note that in the table, vesicle wt% corresponds to the weight fraction of surfactant in vesicle form

Surfactant	Micelle R_g (nm)	Vesicle R_h (nm)	Vesicle wt%	N_{agg}
$C_{12}E_5Ac$ – Slow	1.82 ± 0.06	26 ± 2	1.55 ± 0.06	197
$C_{12}E_5Ac$ – Fast	1.71 ± 0.09	26	0.10 ± 0.01	96
$C_{12}E_5Ac$ – Reverse	1.71 ± 0.07	26	0.03 ± 0.01	96
$C_{13}E_7Ac$ – Slow	1.58 ± 0.13	26	0.14 ± 0.01	51
$C_{13}E_7Ac$ – Fast	1.62 ± 0.04	26	0.10 ± 0.01	58
$C_{18:1}E_5Ac$ – Slow	2.20 ± 0.03	26	0.15 ± 0.02	162
$C_{18:1}E_5Ac$ – Fast	2.18 ± 0.04	26	0.01 ± 0.02	156

Prior to the addition of the base, all of the surfactants show scattering characteristic of very large, locally flat structures such as bilayers or vesicles. This is consistent with previous scattering experiments[18,21] and transmission electron microscopy studies.[16] The initial pH of each of the initial solutions is approximately 2.6, corresponding to a degree of ionisation of 7%.

In Fig. 2b and c, it can be seen that the effects of base-addition-rate are much less pronounced in other, analogous, surfactants. Both the $C_{13}E_7Ac$ and $C_{18:1}E_5Ac$ solutions exhibit a slight upturn at $Q \sim 10^{-1}$ Å^{-1}, indicating the presence of a small fraction of 'larger' structures. This feature is however, very weak compared to the one observed for the $C_{12}E_5Ac$ slow-addition sample and the influence of the addition rate is barely perceptible. To highlight the differences between the samples, the ratio of the intensities from the fast and slow additions are compared in Fig. S4 (ESI†). Note that for the $C_{12}E_5Ac$ and $C_{13}E_7Ac$, the addition speed also appears to affect the shape of the micelles.

To examine the reversibility of the addition-rate effect, a further two $C_{12}E_5Ac$ solutions were prepared;

• Slow-addition of NaOD → addition of DCl → fast-addition of NaOD

• Fast-addition of NaOD → addition of DCl → slow-addition of NaOD

The SANS data from these samples is shown in Fig. S5 (ESI†). Two effects are immediately clear on comparison with Fig. 2a. Firstly, the nanostructures resulting from the two preparation routes are identical *i.e.* the addition-rate effect is no longer present. Secondly, the low-Q region is flat *i.e.* there are no-longer any larger structures in solutions. Both effects have been ascribed to the presence of an inert salt, in this case NaCl, formed by the neutralisation of HCl and NaOH (25 mM, – *i.e.* a slight molar excess with respect to the surfactant), screening the charged headgroups. The same effects are also observed by light scattering when NaCl is added either before or after the addition of NaOH (see Section 3.2.4). This strongly suggests that electrostatic interactions are key to understanding the morphology and stability of the self-assembled aggregates and ultimately, the underlying cause of the addition-rate effect.

3.2 Light scattering

The effects observed by small-angle scattering were investigated in further detail using light scattering methods. The DLS data are presented in three forms: the first-order field correlation function, an inverse Laplace transformation of the correlation function and the parameters resulting from fits of the correlation function to a bimodal exponential model of the form:

$$g^{(1)}(\tau,Q) = A\exp(-D_1Q^2\tau) + (1 - A)\exp(-D_2Q^2\tau) \quad (2)$$

where A and $(1 - A)$ are the relative intensity contributions from components 1 and 2 respectively. The weight fractions of each component can then be obtained by taking into account the respective volumes of the scatterers.[29] The first-order field correlation function provides a clear and objective indication with regards to the presence and relative intensity of different modes in the sample. The inverse Laplace transform[26] yields an intensity-weighted size-distribution, providing information on the sizes and relative amounts of the structures in solution. Finally, fits of the correlation function are used to give quantitative estimates regarding the relative amounts of surfactant present in each type of structure.‡

3.2.1 Surfactant composition. Fig. 2(d–f) shows typical DLS correlation functions, at a scattering angle of 90°, exhibited by high-pH aqueous solutions of $C_{12}E_5Ac$, $C_{13}E_7Ac$ and $C_{18:1}E_5Ac$ respectively. Despite the similar composition of the surfactants, the effect of the base addition-rate is clearly very different. In general, the results agree well with the observations from the small-angle scattering experiment; the $C_{12}E_5Ac$ solutions shows a very pronounced addition-rate effect, whereas the $C_{13}E_7Ac$ and $C_{18:1}E_5Ac$ solutions do not. The data show that the $C_{13}E_7Ac$ solutions do exhibit a slight rate-dependence, however the difference between the calculated weight fractions, as determined from the bimodal fit, is exceedingly small (~0.06%). The $C_{18:1}E_5Ac$ solutions exhibit no rate-dependent behaviour at all and the entirety of the surfactant is micellar form. At this point, it is also noting that the light scattering and neutron scattering techniques are each sensitive to slightly different aspects of the sample, as can be observed in Fig. 2. The intensity of the correlation function scales with the 6th power of the particle diameter and is therefore very sensitive to the presence of larger particles. SANS, on the other hand, is primarily sensitive to the volume of the scattering material and therefore the presence of vesicles is not highlighted as strongly. This effect can be seen in Fig. 2a and d. In Fig. 2d, the

‡ From the SANS results, it can be seen that there is a structure factor peak, which has been ascribed to electrostatic interactions between the smaller, micellar components. To account for this, in each case a structure factor correction, $1/S(Q \to 0)$, has been applied to the smaller of the radii obtained by DLS as quoted in the text.

vesicle mode in the slow addition dominates the intensity, even though it only accounts for 2% of the surfactant volume. In Fig. 2a, the presence of vesicles can be seen by the upturn in intensity at low Q. For the fast and reverse addition samples, the amount of surfactant in vesicle form is approximately 50× less. In the DLS data, the vesicle modes are still clearly visible (even though only 0.1% of the sample is in vesicle form) whereas in the SANS data, this contribution is lost in the noise.

3.2.2 Base concentration, composition and addition rate. In order to determine whether the rate dependence is a continuous phenomenon or rather a threshold effect, high pH solutions of $C_{12}E_5Ac$ were prepared, applying a range of addition rates from 3.7×10^{-7} eq. s^{-1} to 2.8×10^{-3} eq. s^{-1}. Furthermore, to ascertain the influence of the base concentration on the final nanostructures, repeat measurements were conducted with 0.1 M, 1 M and 10 M NaOH. Representative correlation functions and the corresponding size distributions for the 1 M addition (at $\theta = 90^\circ$) are shown in Fig. 3. It is evident, from both plots, that the relative fraction of larger structures decreases with increasing addition rate. This suggests that the effect is continuous rather than threshold-dependant in nature. It can also be seen that at the very slow addition rate, 3.7×10^{-8} eq. s^{-1}, approximately 40% of the surfactant is in vesicle form.

In Fig. 4a, the weight fraction of surfactant in vesicle form (based on eqn (2), full calculations shown in the ESI†) is shown for each base concentration and addition rate. Despite the variability in the data, the trend is again clear; the faster the addition rate of NaOH, the fewer larger structures are present in solution. The weight fractions of surfactant in vesicle form for the 2.8×10^{-3} eq. s^{-1} and 3.7×10^{-6} eq. s^{-1} additions of 1 M NaOH, as calculated from the DLS data, were found to be 0.06% and 2.2% respectively. This agrees well with the weight fractions found by SANS, as given in Table 3. Fig. 4b, shows the mean aggregation number as calculated from the plateau region of the static light scattering data (tabulated values are given in Table S2, SLS data are shown in Fig. S7, ESI†), and confirms the trends and sizes observed from the DLS data. For completeness, the mean aggregation numbers were also calculated from the SANS fit parameters in Table 3, the results (95 and 197 for the 2.8×10^{-3} eq. s^{-1} and 3.7×10^{-6} eq. s^{-1} of 1 M NaOH respectively) are broadly in agreement with the SLS data (46 and 167 respectively) and confirm that all three scattering techniques are showing a consistent, reproducible picture.

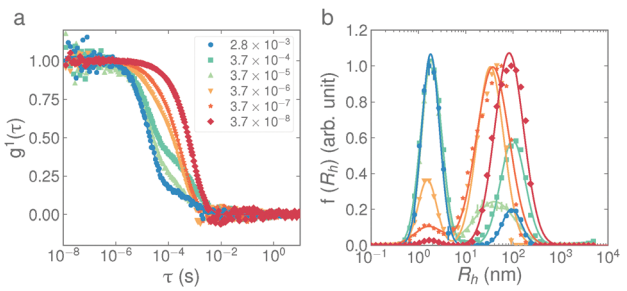

Fig. 3 (a) DLS correlation functions from 1 wt% solutions of $C_{12}E_5Ac$ after the addition of 1 M NaOH at various addition rates. The solid lines in (a) relate to the inverse Laplace transformations and the corresponding intensity-weighted size distributions are shown in (b).

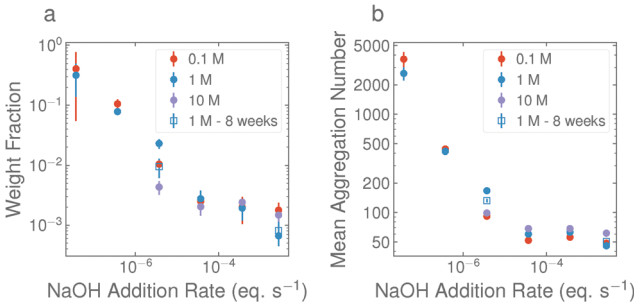

Fig. 4 (a) Weight fractions of surfactant in vesicle form in 1 wt% solutions of $C_{12}E_5Ac$ after the addition of NaOH at various concentrations and addition rates. Plots show an average of all measurements in the range 30°–150°. The weight fractions calculated at 30°, 90° and 150° are shown in Fig. S6 (ESI†). The values are calculated from fits to the bimodal exponential model in eqn (2) taking into account the relative volumes of the scatterers. (b) The mean aggregation numbers as calculated from the plateau of the corresponding static light scattering data (shown in Fig. S7, ESI†).

For the 0.1 M and 1 M solutions, the base concentration appears to have little effect on the final structures. The suppression of larger structures in the case of the 10 M addition may be explained by considering the mechanics of the addition itself. The base was delivered *via* a 21 G needle (with a nominal inner diameter of 0.5 mm), which, due to the surface tension of the base at the tip of the needle, produces droplets with an average volume of ~10 μL. In the case of the 10 M base, only 50 μL is added in total, equating to approx. 5 discrete drops. As a result of this 'discretization', the slower additions were in-fact a composed of a small number of very fast additions.

Finally, the influence of the base cation on the final nanostructure was investigated by performing the equivalent 'fast' and 'slow' additions (2.8×10^{-3} eq. s^{-1} and 3.7×10^{-6} eq. s^{-1} respectively) with KOH replacing NaOH. The results, given in Fig. S8 (ESI†), show that replacing the Na^+ cation by K^+ has little influence on the addition-rate effect, *i.e.* it appears not to be ion specific.

3.2.3 Long-term stability of structures in solution. To examine whether the addition-rate effect persists over longer periods, the NaOH 'fast' and 'slow' addition samples were remeasured after an interval of 60 days. It is clear from Fig. 5 that the structures are remarkably stable and have not converged to a single, thermodynamically stable population over this period. Examining Fig. 5b in further detail, it appears that the fast-addition sample has undergone no significant changes either in the size or the relative amounts of the self-assembled structures. The slow-addition sample exhibits a small increase in the relative amount of smaller structures with respect to larger structures. This difference is small in terms of the calculated weight fractions of surfactant in vesicle form (2.2% *vs.* 0.9%), however it does suggest that the presence of a substantial fraction of surfactant in the form of larger aggregates is not favourable at high pH. The same trend is also observed in the mean aggregation number as calculated from the SLS data (see Fig. 3). Assuming an

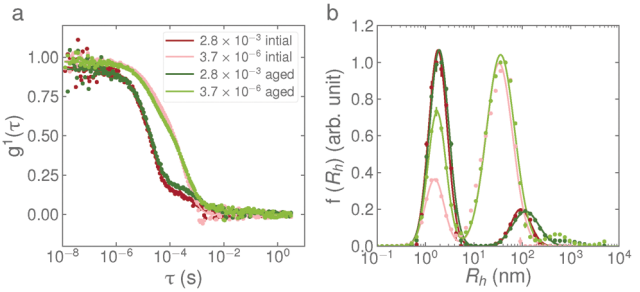

Fig. 5 The DLS correlation functions (a), the corresponding intensity-weighted size distribution functions (b) from the same samples measured immediately after the addition of 1 M NaOH (red, pink) and 8 weeks after the first measurement (dark green, light green).

exponential relaxation of the type: $N_v \sim \exp(-t/\tau)$, one finds the characteristic relaxation time to be approximately 70 days. This is a similar timescale to that observed for the formation of vesicles consisting of anionic and cationic surfactant mixtures.[30] It should be noted that in this specific catanionic system, the vesicles appear to be an equilibrium structure; when additional cationic surfactant is added to the solution, a rapid (<200 ms) vesicle to micelle transition occurs.

3.2.4 Salt effects. As observed in the SANS data, both in this work (Fig. S5, ESI†) and previously,[21] (data reproduced in Fig. S9b, ESI†) the presence of NaCl, appears to suppress the presence of larger aggregates at high pH. The abundance of sodium present in the as received surfactant, was quantified by conducting inductively coupled plasma mass spectrometry measurements (ICP-MS) and was found to be 0.8 ppm. This equates to a concentration in solution of 1 mM and a molar ratio of approx. 21 : 1, surfactant : salt. Light scattering measurements, taken at total salt concentrations of 6 mM and 21 mM§ (*i.e.* molar ratios of approx. 4 : 1 and 1 : 1, surfactant : salt, respectively), are shown in Fig. 6. It can be seen that even at low concentrations, the presence of additional NaCl completely suppresses the appearance of larger structures at high pH and nullifies the addition-rate effect. The calculated diffusion coefficient of the structures is systematically affected by the presence of NaCl, decreasing from an initial value of D = 15.3 (10^{-12} m^2 s^{-1}) in the absence of NaCl to 12.7, 10.7 and 8.5 in the presence of 6 mM (*i.e.* a molar ratio of 4 : 1, surfactant : salt), 21 mM (1 : 1, surfactant : salt) and 100 mM (1 : 4.5, surfactant : salt) NaCl respectively. This effect is most likely due to a decrease in the structure factor contribution, $S(0)$, as the screening of micelle charges is increased. Curiously, when the NaCl is added after the addition of NaOH, it does not immediately disrupt the vesicles already present in solution but does act to reduce the relative amount of vesicles over time (see Fig. 6d) with a characteristic relaxation time of approximately 3 days.

3.2.5 Surfactant purification. In order to ascertain whether the addition-rate effect is related to the presence of impurities in the as-received surfactant, an aliquot of $C_{12}E_5Ac$ surfactant was purified *via* two successive cloud point separations (CPS). Briefly, this was carried out by heating a 5 wt% aqueous surfactant solution to 65 °C in a water bath for two hours. The viscous, surfactant-rich phase was then extracted and dried under vacuum for 16 hours. This process was then repeated. A comparison of the DLS correlation functions and the corresponding size distribution functions for the as received and purified surfactant is presented in Fig. 7. Not only is the addition-rate effect clearly in evidence, the fraction of surfactant material in vesicle form is increased for both 'fast' and 'slow' addition rates. In addition, the hydrodynamic radius of the micelles, R_h = 3.3 nm, is smaller than in the as received samples. From the electrospray ionization mass spectra (shown in Fig. S2 in the ESI†), it appears that the CPS process has not dramatically altered the chain length distribution. The observed effects cannot, therefore, be attributed to any changes

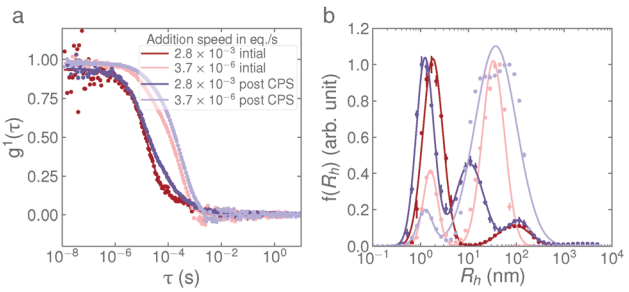

Fig. 7 The DLS correlation functions (a) and corresponding intensity-weighted size distribution functions (b) from 1 wt% solutions of as received and purified $C_{12}E_5Ac$ after the addition of 1 M NaOH.

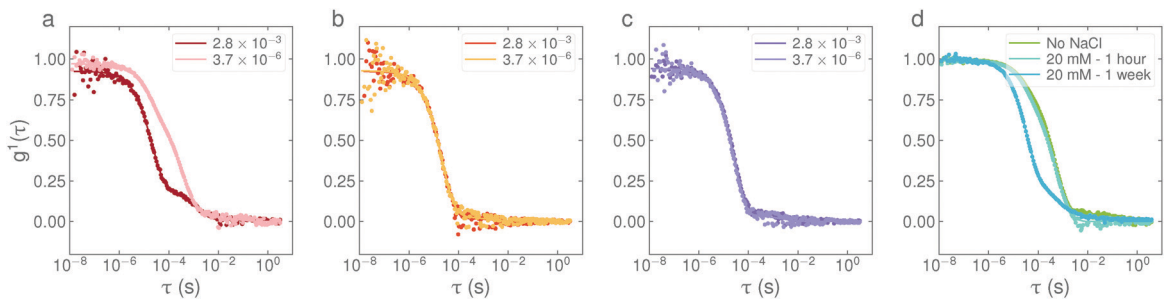

Fig. 6 DLS correlation functions following the fast and slow addition of NaOH to 1 wt% solutions of $C_{12}E_5Ac$ in deionized water (a), 6 mM NaCl solution (b) and 21 mM NaCl solution (c) measured after 8 weeks. Plot (d) shows the effect of adding NaCl to a sample prepared in deionized water after the pH had already been increased at an addition rate of 3.7 × 10^{-6} eq. s^{-1}. Where present, the NaCl concentration in (d) is 21 mM.

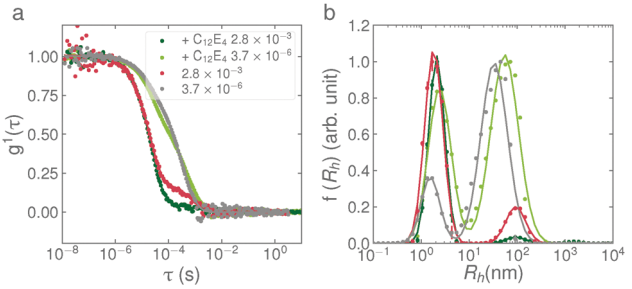

Fig. 8 DLS correlation functions (a) and the corresponding size distribution functions (b) from 1 wt% solutions of $C_{12}E_5Ac$ with an additional 10% of $C_{12}E_4$, after the addition of 1 M NaOH. The equivalent results from the unadulterated samples is shown for comparison.

in the surfactant material itself. It is highly likely however, that the repeated extractions will have removed the residual NaCl in the surfactant. Both the increase in the vesicle fraction, and the reduction of the hydrodynamic radius, are consistent with the trends observed on the addition of NaCl, as described in the previous section.

3.2.6 Addition of non-ionic surfactant. To determine whether the addition-rate effect is affected by the presence of non-carboxymethylated molecules (*i.e.* non-ionic surfactant), an aliquot of $C_{12}E_5Ac$ was mixed with $C_{12}E_4OH$ to increase the non-ionic fraction from approx. 10% to approx. 20%. The results are shown in Fig. 8. It is clear that, although the addition-rate effect is still present in the adulterated sample, it is significantly weaker for both the faster and the slower addition rates (*i.e.* the fraction of vesicles is lower in the adulterated sample than in the unadulterated sample in both cases). The presence of non-carboxymethylated molecules can therefore be ruled out as a cause of the addition-rate effect.

3.2.7 Time spent close to the pK_a. Although we have hitherto referred to the observed phenomena as an 'addition-rate effect', it is, in principle, possible that it is related to the time spent in a pH range where micelles and vesicles coexist. Under this hypothesis, when the pH is increased slowly, the sample spends more time in the vicinity of the pK_a of the surfactant, and therefore in a condition favourable for the assembly of long-term stable vesicles. This phenomenon is very similar to that observed in fatty acids.[31,32] At high pH, the vesicles are not expected to be stable, however, as the surfactant is polydisperse (both in alkyl chain length and in the number of ethylene oxide units), a certain fraction may remain stable in vesicle-form up to higher pH values. When the pH is increased quickly, or when the pH is increased before the surfactant is added (*i.e.* reverse addition), the sample spends little time (or no time at all, in the case of reverse addition) in the vicinity of the pK_a. Consequently, fewer long-term stable vesicles would form and therefore fewer such structures would be observed at high pH.

This interpretation was tested by preparing surfactant solution samples at pH values in the range 3.5–5.5 and allowing them to remain at this pH for 7 days before rapidly adding the remaining NaOH (*via* a single pipette addition) to bring them up to pH 10. The results of this test are given in Fig. S10 in the ESI.† Although a small increase in the vesicle fraction is observed for the sample maintained at pH 5.5, it is clear that the length of time spent close to the pK_a is not the fundamental cause of the observed addition-rate phenomena.

§ Including the 1 mM present in the as received surfactant.

4 Discussion

The phenomena described above, present something of a conundrum. On the one hand, the presence of a small fraction of unusual aggregates in aqueous solutions of industrial surfactants is far from unheard of. In most cases these could be easily dismissed as impurities or contaminants and would be deemed irrelevant. On the other hand, in this case, it is clear that:

1. The presence or absence of these aggregates depends strongly on the preparation pathway.

2. This effect has been demonstrated on different batches of material using different experimental techniques.

3. The effects are significant (up to 40 wt%), systematic and reproducible.

The mystery is further deepened by the fact that the effects are either much weaker ($C_{13}E_7Ac$) or not found at all ($C_{18:1}E_5Ac$) in closely related materials of the same surfactant class. The pathway dependence appears not to be an ion-specific effect, as demonstrated by the near-identical findings with KOH and NaOH, but certainly has an ionic character, as shown by the absence of the effect in the presence of NaCl. Furthermore, the effect only diminishes very slowly, with a characteristic relaxation time of approximately 70 days, does not disappear on heating and cooling and is enhanced by the removal of water-soluble impurities. These observations do not lend themselves easily to a straightforward explanation or a conclusive interpretation, however, various possibilities are discussed below.

One possible culprit for the existence of two distinct self-assembled morphologies is the chemical polydispersity of the surfactant molecules. The $C_{12}E_5Ac$ material not only contains a mixture of C12, C14 and C16 chains (in the approximate ratio 2 : 1 : 0.25), it also features a broad distribution of EO units (from 2 to 16, see Fig. S2 in the ESI†). The difference in size and solubility between headgroups containing 2 EO units and those containing 16 EO units is substantial and the presence of such a broad distribution will undoubtedly give rise to different self-assembly behaviour than would be present if the chain lengths were monodisperse. Indeed, it has previously been observed that the surfactant $C_{12}E_{10}Ac$ does not form vesicles in aqueous solution, even at low pH.[16,18] Furthermore, an investigation into surfactant mixtures of $C_{18}E_{20}$ and $C_{18}E_{100}$, revealed that although they generally form mixed micelles, the constituent surfactants segregate into separate structures when one of them undergoes a phase change.[33] It is therefore not unreasonable to invoke polydispersity as an explanation for the mixture of vesicles and ellipsoidal micelles present at low pH. However,

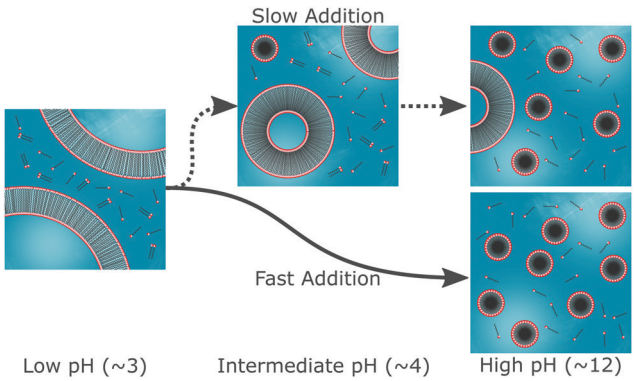

Fig. 9 Schematic summary showing how the rate of change of pH affects the self-assembly behaviour at high pH. In the slow-addition pathway (top) smaller vesicles form at intermediate pH values, in the absence of high NaCl concentrations, these persist as metastable aggregates at high pH. In the fast-addition pathway (bottom) the smaller vesicles disaggregate on addition of NaOH and do not survive to high pH.

polydispersity on its own does not explain the appearance of long-lived vesicles at high pH or the addition-rate effect. It is also worth noting that $C_{13}E_7Ac$, which has a broadly similar (albeit slightly narrower) EO distribution, exhibits only a very weak addition-rate effect.

The pronounced effects of increasing the concentration of NaCl imply that electrostatic interactions play a crucial role in mediating this phenomenon; both those between neighbouring headgroups and those between the surface of the aggregates and the ionic species present in the solution. To understand why this may be the case, it may be instructive to consider the self-assembly process on a molecular level (Fig. 9). The reason why single-chain, weak-acid surfactant molecules can form vesicles, is thought to be due to their propensity to form 'acid soaps', *i.e.* acid-carboxylate dimers.[13–15] The formation of vesicles tends to be centred on the pK_a of the surfactant, as this is the point at which there is an equivalent amount of acidic and anionic surfactant molecules present in solution.[16] Acid soaps are also found in the analogous case of fatty acids, where the formation of stable vesicles is only observed in this pH range.[31,32] The hydrogen-bond between the resulting dimers can be very strong and has been shown to play a significant role in the self-assembly behaviour of *n*-alkyl carboxylic acids.[34] In addition, bilayers or vesicles composed of acid-carboxylate dimers are anionic and have the capacity to sequester cations. This means the local pH in the vicinity of the vesicles may be up to 3 units below that of the bulk.[35] The presence of acid-anion dimers therefore offers some clues regarding the longevity of vesicles up to higher pH values than might otherwise be expected.

Clearly, the above explanation is not complete. As the pH increases, the carboxylic headgroups of the surfactant should become deprotonated and the fraction of dimerised species should decrease. This, in turn, should lead to an increase in the electrostatic repulsion between the headgroups and naïvely, one would therefore expect all of the vesicles to eventually break apart. Despite extensive experimental efforts, the reasons why this does not occur when the pH is changed very slowly, are unclear. Furthermore, the acid-carboxylate hypothesis cannot explain the effect of NaCl on the self-assembly process. When NaCl is present prior to the addition of the base, even in small concentrations, it eliminates the presence of vesicles at high pH. However, it was seen in ref. 21 that when NaCl is present at low pH, it appears to initially promote the presence of monodisperse vesicles, before subsequently suppressing them at high pH (SANS data reproduced in Fig. S9, ESI†). These observations suggest that NaCl stabilises the vesicles at low pH but lowers the activation energy for vesicle disintegration at high pH.

5 Conclusions

It is postulated that these effects arise from a combination of the polydispersity in the length of the EO block and the propensity of single chain weak-acid surfactants to form acid-carboxylate dimers – a phenomenon also found in fatty acids.[31,32] It is known that in conditions close to the pK_a of the surfactant, the formation of stable vesicles occurs, however we have also shown that the effect is not simply related to the amount of time spent close to the pK_a. Rather, the important parameter is the rate of change of pH; by slowing down the addition rate, a substantial fraction of vesicles (up to 40 wt%) is preserved. As the pH increases, the vesicle-to-micelle transition becomes inhibited and at pH 10, the structures are kinetically trapped in vesicle form with a relaxation time of approximately 70 days. The presence of NaCl facilitates the vesicle-to-micelle transition, potentially by disrupting the acid-carboxylate bond. This is not a complete explanation and further work is required to identify the exact mechanisms underlying this phenomenon. However, this effect could be very interesting both from a fundamental physical chemistry standpoint (*e.g.* as a model system to probe the vesicle-to-micelle transition) as well as from an applications perspective (*e.g.* as a mechanism for controlling the encapsulation and delivery of vesicle-borne cargo).

Conflicts of interest

There are no conflicts to declare.

Acknowledgements

The authors gratefully acknowledge the ILL for the allocated beamtime and the Partnership for Soft Condensed Matter (PSCM) for the use of their instruments. D. W. H. was supported by BMBF grant [05K16KT1] and L. C. acknowledges the TU-Berlin and the ILL for postdoctoral funding through a three-year cooperation agreement.

References

1 K. Holmberg, B. Jönsson, B. Kronberg and B. Lindman, *Surfactants and Polymers in Aqueous Solution*, John Wiley & Sons, Ltd, Chichester, UK, 2002.
2 E. A. G. Aniansson, S. N. Wall, M. Almgren, H. Hoffmann, I. Kielmann, W. Ulbricht, R. Zana, J. Lang and C. Tondre, *J. Phys. Chem.*, 1976, **80**, 905–922.

3 A. Shioi and T. A. Hatton, *Langmuir*, 2002, **18**, 7341–7348.
4 J. Leng, S. U. Egelhaaf and M. E. Cates, *Europhys. Lett.*, 2002, **59**, 311–317.
5 T. M. Weiss, T. Narayanan, C. Wolf, M. Gradzielski, P. Panine, S. Finet and W. I. Helsby, *Phys. Rev. Lett.*, 2005, **94**, 1–4.
6 K. Bressel, M. Muthig, S. Prevost, J. Gummel, T. Narayanan and M. Gradzielski, *ACS Nano*, 2012, **6**, 5858–5865.
7 R. G. Laughlin, *Colloids Surf., A*, 1997, **128**, 27–38.
8 E. Feitosa, G. Karlsson and K. Edwards, *Chem. Phys. Lipids*, 2006, **140**, 66–74.
9 V. Guida, *Adv. Colloid Interface Sci.*, 2010, **161**, 77–88.
10 H. Madani and E. W. Kaler, *Langmuir*, 1990, **6**, 125–132.
11 Y. Talmon, D. F. Evans and B. W. Ninham, *Science*, 1983, **221**, 1047–1048.
12 J. E. Brady, D. F. Evans, B. Kachar and B. W. Ninham, *J. Am. Chem. Soc.*, 1984, **106**, 4279–4280.
13 P. Walde, M. Wessicken, U. Rädler, N. Berclaz, K. Conde-Frieboes and P. L. Luisi, *J. Phys. Chem. B*, 1997, **101**, 7390–7397.
14 T. Sakai, M. Miyaki, H. Tajima and M. Shimizu, *J. Phys. Chem. B*, 2012, **116**, 11225–11233.
15 T. Sakai, R. Ikoshi, N. Toshida and M. Kagaya, *J. Phys. Chem. B*, 2013, **117**, 5081–5089.
16 A. Renoncourt, P. Bauduin, E. Nicholl, D. Touraud, J. M. Verbavatz, M. Dubois, M. Drechsler and W. Kunz, *ChemPhysChem*, 2006, **7**, 1892–1896.
17 N. Vlachy, C. Merle, D. Touraud, J. Schmidt, Y. Talmon, J. Heilmann and W. Kunz, *Langmuir*, 2008, **24**, 9983–9988.
18 L. Chiappisi, *Adv. Colloid Interface Sci.*, 2017, **250**, 79–94.
19 H. W. Stache, *Anionic Surfactants: Organic Chemistry*, Taylor & Francis, 1995.
20 G. Czichocki, H.-R. Holzbauer and C. Martens, *Fett Wiss. Technol.*, 1992, **94**, 66–73.
21 D. W. Hayward, L. Chiappisi, S. Prévost, R. Schweins and M. Gradzielski, *Sci. Rep.*, 2018, **8**, 7299.
22 D. Leinweber, U. Dahlmann and R. Kupfer, *Process for the solvent-free preparation of ethercarboxylic acids having a low residual salt content*, *US Pat.* 7208118, 2007.
23 T. A. Cripe, *Process for making alkyl ethoxy carboxylates*, *US Pat.* 5233087, 1993.
24 P. Lindner and R. Schweins, *Neutron News*, 2010, **21**, 15–18.
25 D. W. Hayward, L. Chiappisi, S. Prévost and R. Schweins, Internal time on D11, 2017, DOI: 10.5291/ILL-DATA.INTER-354.
26 S. Hansen, *Eur. Biophys. J.*, 2018, **47**, 179–184.
27 H. Oikawa, *Polymer*, 1992, **33**, 1116–1119.
28 A. J. F. Siegert, *On the fluctuations in signals returned by many independently moving scatterers*, Radiation Laboratory, Massachusetts Institute of Technology, 1943.
29 M. Shibayama, T. Karino and S. Okabe, *Polymer*, 2006, **47**, 6446–6456.
30 S. Bucak, B. H. Robinson and A. Fontana, *Langmuir*, 2002, **18**, 8288–8294.
31 K. Fontell and L. Mandell, *Colloid Polym. Sci.*, 1993, **271**, 974–991.
32 P. Walde, T. Namani, K. Morigaki and H. Hauser, *Liposome Technology*, Informa Healthcare, 2006, vol. I, pp. 1–19.
33 B. Plazzotta, J. Dai, M. A. Behrens, I. Furó and J. S. Pedersen, *J. Phys. Chem. B*, 2015, **119**, 10798–10806.
34 R. Smith and C. Tanford, *Proc. Natl. Acad. Sci. U. S. A.*, 1973, **70**, 289–293.
35 T. H. Haines, *Proc. Natl. Acad. Sci. U. S. A.*, 1983, **80**, 160–164.